Plasma Jet Driven Magneto-Inertial Fusion

(PJMIF)

Y. C. Francis Thio,[*,a] Scott C. Hsu,[b] F. Douglas Witherspoon,[a,c] Edward Cruz,[a] Andrew Case,[a,c] Samuel Langendorf,[b] Kevin Yates,[b,g] John Dunn,[b] Jason Cassibry,[d] Roman Samulyak,[e] Peter Stoltz,[f] Samuel J. Brockington,[a,c] Ajoke Williams,[a,c] Marco Luna,[a,c] Robert Becker,[a] and Adam Cook[a]

[a] *HyperJet Fusion Corporation, Chantilly, VA 20151*

[b] *Physics Division, Los Alamos National Laboratory, Los Alamos, NM 87545*

[c] *HyperV Technologies Corp., Chantilly, VA 20151*

[d] *University of Alabama in Huntsville, Aerospace and Mechanical Engineering Department Huntsville, AL*

[e] *Brookhaven National Laboratory, NY*

[f] *Tech-X Corporation, Denver, Colorado*

[g] *Electrical and Computer Engineering Department, University of New Mexico, Albuquerque, NM 87131, USA*

[*]Email: francis.thio@hyperjetfusion.com

Number of pages: 32
Number of tables: 7
Number of figures: 10

Abstract

PJMIF is the only embodiment of magneto-inertial fusion that has the unique combination of standoff implosion and high implosion velocity (50 km/s - 150 km/s). It uses inexpensive plasma guns for all plasma formation and implosion. It has potential for relatively high repetition rate from 1 to 2 Hz. Its configuration is compatible with the use of a thick liquid wall that doubles as a tritium breeding blanket as well as a coolant for extracting the heat out of the fusion reactor. Its operational parameter space allows for the possibility of using a sufficiently dense target plasma for the target plasma to have a high β. If such a high β plasma could be realized, it would help to suppress micro and MHD instabilities, giving its target plasma classical transport and energy confinement characteristics. Its open geometry and moderate time and spatial scales provide convenient diagnostics access. Diagnostics accessibility, high shot rate and low cost per shot should enable quick resolution of technical issues during development, thus the potential for enabling rapid R&D of PJMIF. There are a number of challenges, however, for PJMIF including being at a very early stage of development, developing the required plasma guns, dealing with potential liner non-uniformities, clearing the chamber of residual high-Z gas between shots, and developing the repetitive pulsed power component technologies. Over the last three years, the development of the Plasma Liner Formation Experiment (PLX-α) have been undertaken to explore the physics and demonstrate the formation of a spherical liner by the merging of a spherical array of plasma jets. Two- and three- jet merging experiments have been conducted to study the interactions of the jets. Six- and seven-jet experiments have been performed to form a piece of the plasma liner. A brief status report on this development is provided in this paper.

Keywords — Plasma jet, Magneto-inertial fusion, Pulse coaxial plasma guns, Slab-mode, Fusion, Reactor concept, Innovative Fusion Approaches, PLX, Plasma liner, ARPA-E ALPHA

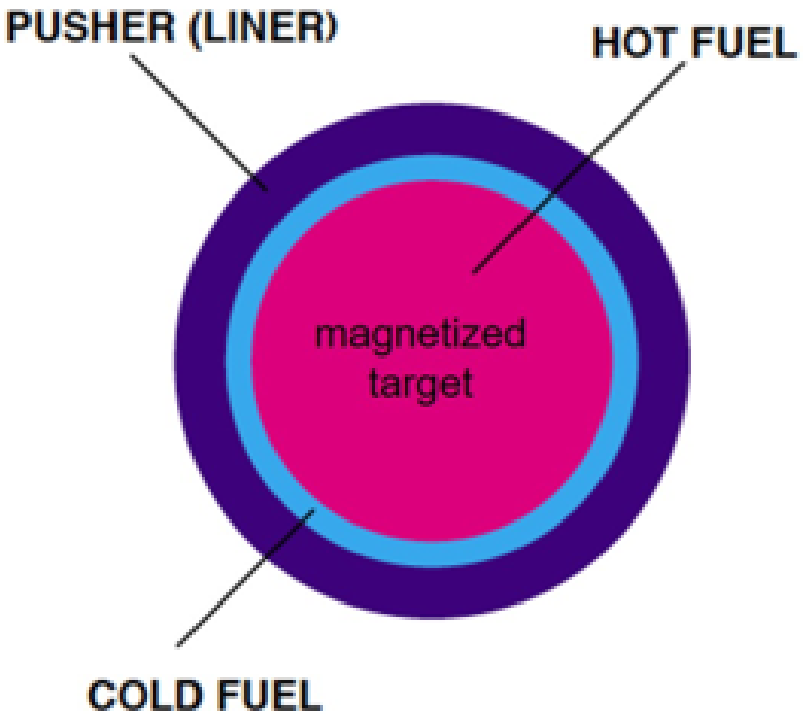

Fig. 1. In magneto-inertial fusion (MIF), a heavy pusher (liner) is used to compress a magnetized plasma target. The liner may be solid, liquid, or gaseous. Sometimes a cold fuel layer is used to boost the fusion gain of the configuration

I. INTRODUCTION

PJMIF is one of several possible embodiments of magneto-inertial fusion, an emerging class of modern fusion approaches. In magneto-inertial fusion (Figure 1), a magnetized plasma target is imploded by a material shell, called a liner. The target plasma is preheated to a sufficiently elevated temperature, typically $\sim 100-300$ eV (about 1 - 3 million degrees Kelvin), so that radial convergence of the liner-on-target implosion may be limited to be less than 10 to limit the degree of hydrodynamic instabilities during the implosion. The liner may be solid, liquid or gaseous. MIF is indeed a hybrid of magnetic and inertial fusion. Just as in magnetic fusion, the magnetic field in the target suppresses thermal transport in the plasma. On the other hand, just like inertial fusion, it employs compression to heat the fusion fuel efficiently, and the burning plasma is kept away from the wall of the chamber. Compared to the ablator in pure inertial fusion, the mass of the liner is relatively large and significantly extends the containment time of the burning plasma, a feature not present in pure inertial fusion. This allows magneto-inertial fusion to obtain reasonable fusion gain with orders of magnitude lower plasma density than pure inertial fusion. Due to the suppression of the thermal transport by the magnetic field, much lower implosion velocity is possible in MIF to produce ignition compared with pure inertial fusion.

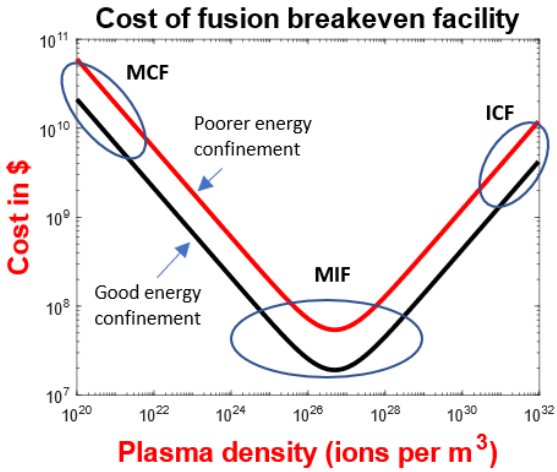

Fig. 2. Results based on Lindemuth and Siemon [1]

All these features combine to make it possible for MIF to produce fusion burn with a density intermediate between the two extremes of magnetic and inertial fusion. In this intermediate density regime, Lindemuth and Siemon, in their celebrated paper of 2009 [1], show that the cost of a fusion breakeven facility might have a minima, as shown in Figure 2. When the density of the burning plasma is low, the size of the plasma is large in order to have sufficiently large Lawson's number, driving up the cost of the fusion reactor. When the plasma density is high, the power of the fusion driver increases, again driving up the cost of the fusion reactor. Magneto-inertial fusion aims at exploiting the sweet spot between the two extremes in density in the fusion parameter space.

In one embodiment of PJMIF [2, 3], Figure 3, two sets of plasma guns are used. One set launches the target jets, from 24 to 60 jets, carrying the fusion fuel and the magnetic flux, at velocities of about 100 km/s. The jets merge and converge towards the center of an evacuated reactor chamber forming a magnetized plasma ball that serves as the target. The self-stagnation of the target plasma ball preheats the target to the desired initial temperature. A second set of plasma guns, as many as 300 to 600 in number, launches the liner jets carrying heavy ions, at velocities ranging from 50 km/s to 100 km/s. The jets merge to form a heavy liner, shown in blue in Figure 3, that continues to converge towards the center of the chamber. At some point during its convergence, the liner compresses the target, raising its temperature and density, as well as compressing the magnetic flux embedded in the target, thus increasing the magnetic field intensity as the implosion proceeds. When the target plasma reaches sufficiently high temperature and density, fusion reactions occur, resulting in a burst of alpha particles and neutrons [2, 4]. If

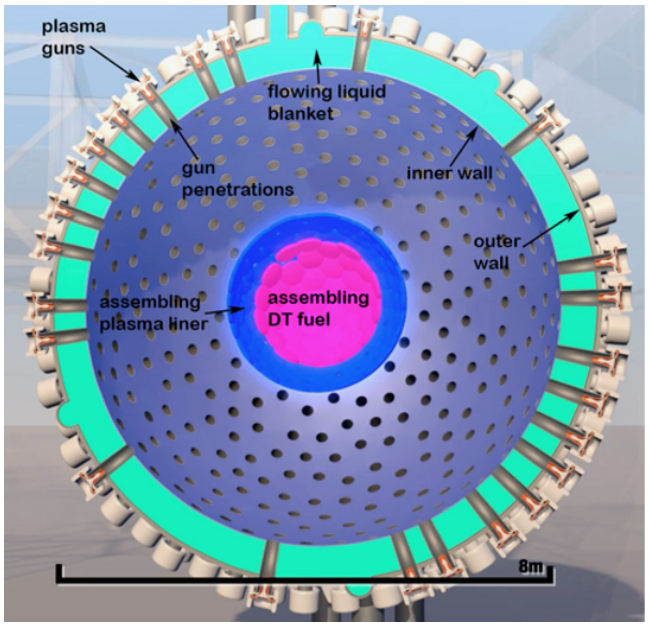

Fig. 3. The PJMIF fusion concept

the magnetic field is sufficiently high, it enhances alpha energy deposition in the target, leading to further heating of the target, increasing the fusion burn rate and the burn fraction of the target, and the target fusion gain. The target fusion yield and gain can be further amplified by the use of a cold afterburner layer of fusion fuel between the liner and the target[2]. This is briefly discussed in Section III.A The alpha particles and the neutrons are absorbed by a circulating liquid blanket. The liquid blanket serves as the coolant as well as a tritium breeding blanket. The cycle is repeated about once a second or two.

An outline of the rest of this paper is as follows. Following the Introduction, the appeal and challenges of PJMIF is described, the potential fusion gain achievable with PJMIF according to two U.S. Department of Energy (DOE) radiative magnetohydrodynamic (MHD) codes are reported, together with the baseline burn configuration of PJMIF. These studies lead to the determination of the requirements of the plasma guns for PJMIF. The requirements of the plasma guns and its state of development is described in Section IV. In Section V, the reactor considerations of the plasma guns and the chamber at reactor scale are discussed. In Section VI, a brief status report of the experiments on jet merging and the formation of a plasma liner is given. This is followed by a brief summary of the paper.

II. THE APPEAL AND CHALLENGES OF PJMIF

PJMIF is the only embodiment of MIF that has simultaneously the attributes of high implosion velocity and standoff. By standoff, we mean the launching of the required implosion momentum and energy at a sufficiently large distance from the nuclear fusion micro-explosion site to avoid significant hardware damage, thus preserving the integrity of the driver for a reasonably large number of shots. High implosion velocity allows smaller and denser targets to be fielded with higher target gain. It provides headrooms for dealing with degradation of thermal transport and energy confinement. It plans to use low-cost plasma guns for all plasma formation and implosion, though at the present time, the ability of assembling a $\beta > 1$ target plasma remains to be demonstrated and is a subject of open research [5]. Work is in progress to conduct two-magnetized-jet merging experiments on the Big Red Ball plasma science facility at U. Wisconsin-Madison to see if we can create transient conditions with $\beta > 1$ and ion Hall parameter $\omega_i \tau_i > 1$. The reactor approach is compatible with the use of thick liquid walls. The standoff delivery of the implosion energy and momentum provide it with the potential for high repetition rate (e.g. 1 Hz). Very high-β target may be used, suppressing micro and MHD instabilities. Its open geometry and moderate temporal and spatial scales increases accessibility for diagnostics. The high degree of diagnostic accessibility, combined with the low-cost nature and high rates of experimental tests, enable rapid resolution of technical issues, and thus potentially enabling rapid and low-cost R&D.

However, there remain a number of challenges for PJMIF. Its development is at a very early stage of development with low TRL (Technology Readiness Level) for both the liner and the target. Plasma guns capable of launching plasma jets with the required properties (see below) remain to be developed. Liner non-uniformities could exacerbate deceleration-phase instabilities, which could lead to liner-target materials mix, and a reduction in the degree of target compression. Chamber clearing of high-Z liner residual gas between shots is non-trivial. Lastly but not the least, repetitive operations and the required pulsed power technologies (switches and capacitors with the required lifetime and energy density) need to be developed.

TABLE I
Baseline Burn Configuration for PJMIF

Target at Peak Compression	
Density	$5 \times 10^{21}\ cm^{-3}$
Temperature	10 keV
Pressure	150 Mbar
Radius	0.4 cm
Mass	5 mg
Magnetic field	300 T
Dwell time	500 ns
Afterburner	
Density	$5\times 10^{22} cm^{-3}$
Mass	20 mg
Liner	
Velocity	70 km/s
Mass (high-Z)	10 g
Kinetic energy	25 MJ
Thickness at stagnation	2 cm
Net fusion gain	20

III. PJMIF GAIN AND BASELINE CONFIGURATION

Burn configurations for PJMIF are selected to capture the sweet spot in the fusion parameter space (Fig. 2), while allowing plenty of headroom in the implosion velocity to mitigate any "surprises" in transport during target implosion and burn. The baseline parameters for a potentially attractive burn configuration is shown in Table I. The exact values of these parameters remain to be optimized as our understanding and the predictive capability of our models increase with further research. The implosion dynamics is designed to achieve this configuration or one that is optimized around it.

III.A. PJMIF reactor parametric study and the two-stage booster concept using an afterburner

Implosion dynamics and burn scenarios to achieve the burn configuration of Table I were designed and modeled by Thio [6] using an idealized 1D Lagrangian fluid code, Lf1d. In Thio [6], the plasma is modeled as an ideal fluid with no thermal conduction to ease the computational burden. For the target plasma and the afterburner, it is assumed that the embedded magnetic fields in these regions are sufficiently strong to suppress the thermal transport and to provide the required degree

of enhancement of alpha deposition specified as an input parameter in the simulation. Modeling the liner without thermal conduction tends to make the liner less compressible and lowers the efficacy of the liner in compressing the afterburner and target. The computed implosion dynamics is thus somewhat on the conservative side due to lack of thermal conduction. On the other hand, the 1D nature of the simulation produces inherently optimistic implosion dynamics.

It is envisaged that the target jets arrive first at the center. After stagnating to form a spherical ball of about 100 eV and relatively low density ($\sim 10^{24}$ ions per m^3), the target rebounds. In the meantime, the plasma guns/accelerators that launch the liner jets carry a small amount of cold, dense DT gas ($\sim$ 1 eV, $\sim 10^{26}$ ions per m^3 ion density) on their noses. When the afterburner and liner engage the target, the cold afterburner is sandwiched by the thermal pressure of the target and the combination of ram and thermal pressure of the liner. When the assembly is complete, the afterburner is in a pressure balance with the target and liner. This assembly is referred to as the configuration at engagement. If the afterburner is sufficiently cold, the pressure balance will cause it to be very thin by design ($\sim$ 1 mm thick), so that the transit time for pressure forces within the afterburner is short compared to the implosion time scale. This allows the ram pressure of the liner to be efficiently transmitted through the afterburner to implode the target. The afterburner also provides a buffer between the high-Z liner and the target to prevent mixing of the high-Z materials with the low-density target. By design, the afterburner is two orders of magnitude colder than the target, its density is about two orders of magnitude higher. By virtue of its high density, the afterburner is less vulnerable to the high-Z mixing from the liner than the target if the target is in direct contact with the high-Z liner. Also only a very thin inner layer of the afterburner needs to be ignited. The issue of the actual assembly of such a configuration and the requisite magnetization of the target and afterburner is a subject for future investigation and development. Existing plasma jet technology and magnetization techniques are not yet capable of producing these configurations. Development of new plasma gun/accelerator technologies and plasma magnetization techniques is needed.

The afterburner is a two-stage booster concept. The target plasma is ignited first by the implosion. A fraction of the fusion energy generated by the target is then used to heat and ignite the afterburner. For this to occur, two conditions must be satisfied: (1) the target must have sufficiently large fusion yield resulting in a strong burst of alpha energy, (2) a fraction of the alpha

energy must be allowed to escape from the target, i.e. the **alpha escape franction** from the target must be greater than 0.

More than 200 cases were run using the code Lf1d in order to identify a region of the parameter space from which access to ignition is possible. The parameter space is spanned by the spatial dimensions, velocities, density, temperature, magnetic field, and adiabatic indices of the target, the afterburner and the liner. A number of cases were found in which the target fusion gain exceeds 10, and the total fusion gain exceeds 20 [6]. A few illustrative cases are shown in Table II. The target fusion gain is defined as the ratio of the fusion yield from the target to the total energy of the configuration at engagement. A similar definition applies to the total fusion gain which includes the fusion yield from the afterburner.

In each run of Lf1d, the simulation begins by assuming an initial configuration consisting of the target, afterburner and the plasma liner, all in contact with each other. With reference to Table II, Case #170 provides the basis for the baseline burn configuration of Table I. In that run, the target generates a fusion yield of 334.7 MJ, sufficient to heat and ignite the afterburner, which adds another 1,633 MJ to the fusion yield, giving a total fusion yield of 1,967 MJ. The total energy of the initial configuration (which is mostly the kinetic energy of the liner) is 30 MJ. Thus, the target fusion gain is 11.32, and the total fusion gain is 66.5. In this case the target alpha deposition fraction is set to 0.95, thus the alpha escape fraction is 0.05, sufficient to ignite the afterburner. Case #177 is a more optimal case which uses a smaller amount of liner kinetic energy (20 MJ), and a set of less demanding afterburner and liner initial condition: a higher afterburner initial temperature of 1.83 eV, and a higher liner initial temperature of 3.13 eV. This case produces a similar target gain (12.7) and total fusion gain (61.5).

On the other hand, if the alpha energy is completely trapped in the target as in the Case #169 where the alpha deposition fraction in the target is set to 1.0, the afterburner fails to ignite. The afterburner is heated only to a temperature of about 249 eV by compression. Case #163 is a repeat of Case #169 except for the imploding velocity which is reduced to 60 km/s. In this case, the target still ignites, yielding 271.7 MJ of fusion energy, with a target fusion gain of 12.3.

While the actual realization of such an assembly is a subject for future development, it may be checked, however, that the configurations are physically feasible. For example, the initial thermal pressure of the afterburner can be contained by the combination of the thermal and ram

TABLE II
Exemplary cases from rapid scan of PJMIF burn configurations using the Lf1d code. Common values of parameters at engagement for all four cases are as follows. Target: radius 40.6 mm, ion density 4.28×10^{24}, mass 5 mg, temperature 80 eV, thermal pressure 1.1×10^{8} Pa; Afterburner - thickness 1.354 mm, ion density 1.87×10^{26}, mass 22.5 mg; Liner thickness 11.7 mm

Case	#163	#169	#170	#177
At engagement				
Target alpha deposition fraction	1.0	1.0	0.95	0.75
Afterburner temperature (eV)	0.5	0.5	0.5	1.83
Afterburner pressure (Pa)	3×10^{7}	3×10^{7}	3×10^{7}	5.48×10^{7}
Afterburner velocity (km/s)	-60	-70	-70	- 70
Liner mass (g)	12.04	12.04	12.04	8.028
Liner velocity (km/s)	60	70	70	70
Liner temperature (eV)	1.38	1.38	1.38	3.13
Liner ram pressure	1.287×10^{11}	1.762×10^{11}	1.762×10^{11}	1.167×10^{11}
Total energy of configuration (MJ)	21.8	30	30	20
At maximum fusion power				
Target				
Target radius (mm)	3.76	3.463	2.98	2.942
Peak Target density	3.097×10^{27}	9.349×10^{27}	$1.125 \times 10^{2}8$	1.225×10^{28}
Peak temperature (keV)	55	92.75	137	100
Peak pressure	1.12×10^{14}	$1.06 \times 10^{1}4$	4.95×10^{14}	1.58×10^{14}
Target fusion yield	271.7	278.3	334.7	249.7
Afterburner				
Ignition	No	No	Yes	Yes
Thickness (mm)	0.0479	0.098	1.276	1.956
Peak density	8.24×10^{29}	1.22×10^{30}	5.293×10^{28}	4.995×10^{28}
Peak temperature (keV)	0.22	0.249	34.1	32.6
Peak pressure (Pa)	5.31×10^{13}	1.09×10^{14}	2.892×10^{14}	1.569×10^{14}
Afterburner fusion yield (MJ)	4.4	24	1633	964.1
Total Fusion Yield (MJ)	271.7	302	1967	1214
Target fusion gain	12.3	9.4	11.32	12.7
Total fusion gain	12.5	10.2	66.5	61.5

pressures of the target and the liner. In physical realization, the pressures and temperatures will not have the numerical discontinuities indicated by these initial conditions used in the simulations. However, any numerical discontinuities in pressures will be rapidly damped out in the numerical simulations.

III.B. Verification using DOE national laboratory codes

Based on the results and suggestions from the parametric study described above, Knapps and Kirkpatrick [4] undertook a study of possible fusion gain from PJMIF using two DOE national laboratory radiative hydrodynamic codes, where fusion gain is computed as the ratio of the total

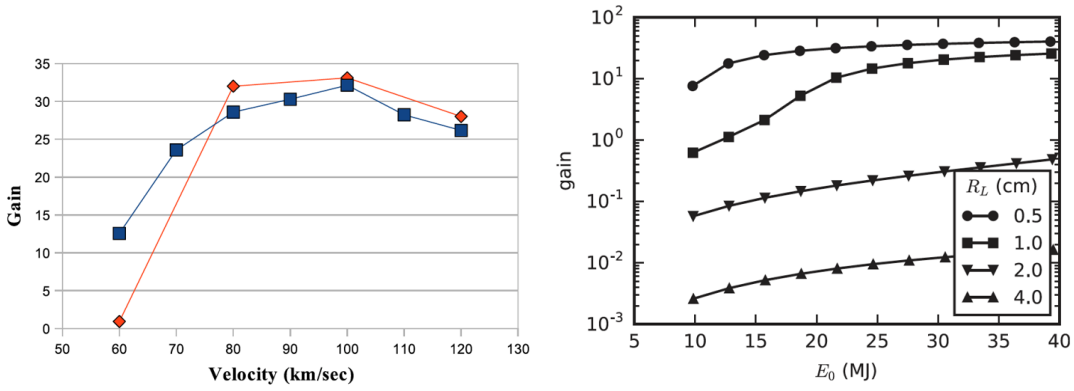

(a) (b)

Fig. 4. Possible PJMIF gain: (a) Results from two DOE national laboratory radiative magneto-hydrodynamic codes; Courtesy of Knapps and Kirkpatrick [4]; (b) Results from a semi-analytical code of Langendorf and Hsu. Courtesy of Langendorf and Hsu [7].

fusion yield to the total initial liner and target energy. The results from these codes (Figure 4(a)) indicate that PJMIF gains greater than 30 are possible with driver energy between 25 – 50 MJ. These results are consistent with results (Figure 4(b)) obtained with a semi-analytical code of Langendorf and Hsu [7] that include models for cross-field transport, fusion burn, alpha deposition, 2-temperature (electrons and ions) and EOS/Radiative effects.

While higher dimensional effects will tend to degrade the fusion performance on the one hand, on the other hand further optimization of the implosion parameters could compensate for the performance degradation. For the purpose of the conceptual reactor design presented in this paper, we will adopt a nominal modest value of 20 for the fusion gain as the baseline.

III.C. Baseline PJMIF Power Reactor Energy Flow

PJMIF is a pulsed fusion approach which generates a continuous power output by repetitive firings of its fusion reactor. Fig. 5 shows the nominal energy flow per shot (firing) of the reactor. A total of 50 MJ of electrical energy is stored among the distributed capacitor modules that drive the plasma guns to produce the plasma jets. Assuming an efficiency of 50% for the plasma guns, the total energy of the plasma jets that merge to form the plasma liner is 25 MJ. With a net fusion gain of 20, the total fusion yield is 500 MJ, of which 100 MJ appears as alpha particles and 400 MJ as kinetic energy of neutrons.

The kinetic energy of the neutrons is thermalized in a lithium-based blanket, and the ther-

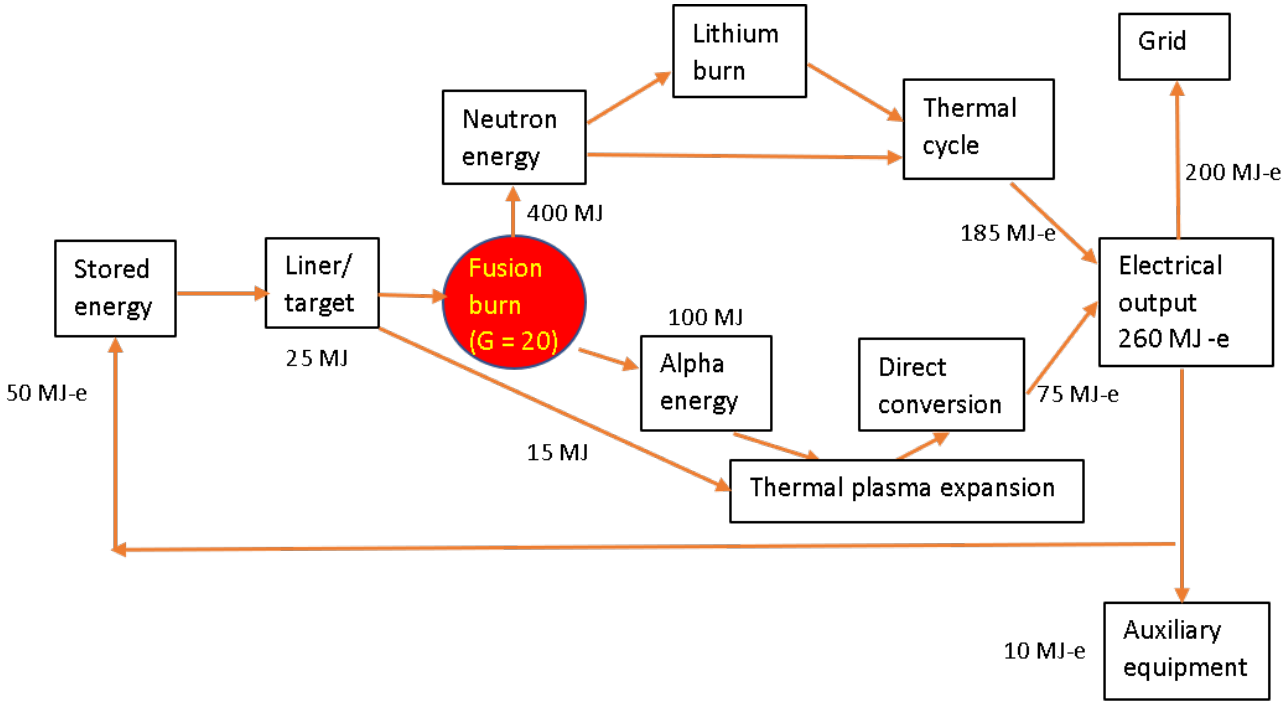

Fig. 5. Baseline energy flow of a PJMIF fusion cycle.

malized neutrons are used to regenerate the tritium via the ${}^{6}_{3}Li({}^{1}_{0}n,{}^{4}_{2}He){}^{3}_{1}T$ reaction, which is exothermic (4.6 MeV per reaction), yielding another 125 MJ of thermal energy. These two neutron processes combine to yield a total of 525 MJ of thermal energy that can be used to drive a standard steam cycle to generate electricity at approximately 35% efficiency, yielding 185 MJ of electrical energy. The kinetic energy of the imploding liner minus the energy radiated is transformed into thermal energy (estimated to be $>$ 15 MJ) of the liner at several 10's eV. Adding to this, the 100 MJ of alpha energy is deposited in the target, the afterburner and a thin inner layer of the liner causing a strong, point-like, micro-nuclear explosion creating a plasma fireball, that expands at sufficiently high speed which can be harnessed to generate electricity by direct energy conversion (DEC, see for example [8]) at high efficiency (we assume 65%). This path generates approximately 75 MJ of electrical energy. The total electrical energy generated by the steam cycle and the direct MHD conversion is thus 260 MJ-e, of which 50 MJ-e is recycled to charge the capacitor modules for the next shot, and 10 MJ-e is used to drive the auxiliary equipment (vacuum system, the liquid wall system, thermal management system, tritium management system, etc.)

TABLE III
Technological demands on the plasma jets

Parameter	Requirement	Achieved
Jet Length	< 5 cm	10 cm core
Velocity	70 km/s	50 km/s
Efficiency	$> 50\%$	30%
Density	1×10^{18} per cc	1×10^{16} per cc
Mach number	> 10	> 10
Jet-to-jet mass variations	$< 5\%$	$< 2\%$ for 7 jets

IV. PLASMA GUN REQUIREMENTS FOR PJMIF AND THE STATE OF ITS DEVELOPMENT

Compact, dense, high-velocity, high-Mach number plasma liners are required for PJMIF, requiring plasma jets of similar compactness, density, velocity and Mach numbers [2, 9, 7]. In addition, a high degree of temporal, spatial and kinetic (energy and momentum) coherence among the jets is required. 3D modeling studies using the FronTier code of Brookhaven National Laboratory on the merging of 6 plasma jets to form a conical section of the liner (see later) show that jet-to-jet mass variations should be kept to be less than 5% in order to limit the degradation on the ram pressure and the uniformity of the liner to be within reasonable limits [10]. For the same reason, variation in the timing of the launching of the jets should be limited to be less than 200 ns. These requirements are summarized in Table III.

There are three modes in which plasmas can be accelerated in coaxial plasma guns: (1) Deflagration, (2) snow-plow, and (3) slab. In deflagration mode, a surface flashover is caused along the insulator surface at the breech by applying a high voltage between the electrodes. An arc is formed and continues to ablate materials off the insulator surface, feeding the arc. The arc is accelerated by the $\mathbf{j} \times \mathbf{B}$ Lorentz force. In this mode, because the plasma is continuously added to the rear of the plasma, this is the mode for creating long plasma jets. In the snow-plow mode, the gun is pre-filled with a gas with the desired atomic species. An electrical breakdown is again caused at the back end of the gas column forming a current sheet by pre-ionizing a thin sheet of the gas and applying a sufficiently high voltage across the current sheet. The electrons in the current sheet carries the current and are accelerated by the Lorentz force $\mathbf{j} \times \mathbf{B}$ and drags the ions along by ambipolar diffusion. The neutrals ahead of the current sheet get ionized by electron impacts and become entrained in and move with the current sheet. This is the 'snow-plow' action of the

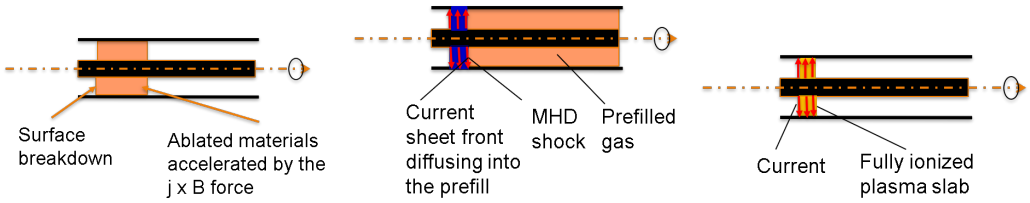

(a) (b) (c)

Fig. 6. Three modes of plasma acceleration in a coaxial plasma gun: (a) Deflagration, (b) Snow-plow, (c) Slab or washer mode

current sheet, gathering up the neutrals in front of it, after the neutrals become ionized.

If the ionization of the neutrals is not 100%, some of the neutrals will be left behind. These neutrals may become ionized subsequently and add to the length of the plasma tail. They are also agents for promoting restrikes behind the main plasma armature. Thus, both the deflagration and snow-plow modes of plasma acceleration in a coaxial plasma gun are not suitable as a driver for PJMIF. In addition, in the snow-plow mode, acceleration of the ion ceases when the velocity of the neutrals in the frame of the advancing current sheet reaches a value corresponding to its ionization energy. The collision kinetic energy between the particles are absorbed as the ionization energy of the neutrals. The effect limits the acceleration of the current sheet to below a velocity known as the Alfven's critical ionization velocity.

The slab mode is the mode that has the potential for launching plasma jets needed for plasma liner formation [11]. The key here is fast gas injection to form an initial gas slab detached from any insulator surface between the gun electrodes. The initial gas slab is pre-ionized by some appropriate means (see later for an example) to form a compact, dense, and highly collisional plasma. The slab mode of coaxial plasma acceleration is vulnerable to the blow-by instability [12]. To avoid the blow-by instability, Thio [13, 14] proposed the contouring of the electrodes to induce a radial density profile in the plasma slab to better match the magnetic pressure profile. The concept of the contoured-gap electrodes was first reduced to practice at HyperV Technologies in 2009 [15].

Under the ARPA-E ALPHA program launched in 2015, a plasma gun, called the ALPHA2gun was developed. The ALPHA2gun has six principal features (Fig. 7): (a) A gas valve that opens and closes in about $600\mu s$, (b) a set of 20 capillary injectors (miniature electrothermal guns) to pre-ionize the initial gas slab, (c) the contoured coaxial gun electrodes to suppress the blow-by instability, (d) a capacitor bank consisting of 6 submodules of 100 μF capacitors with low-

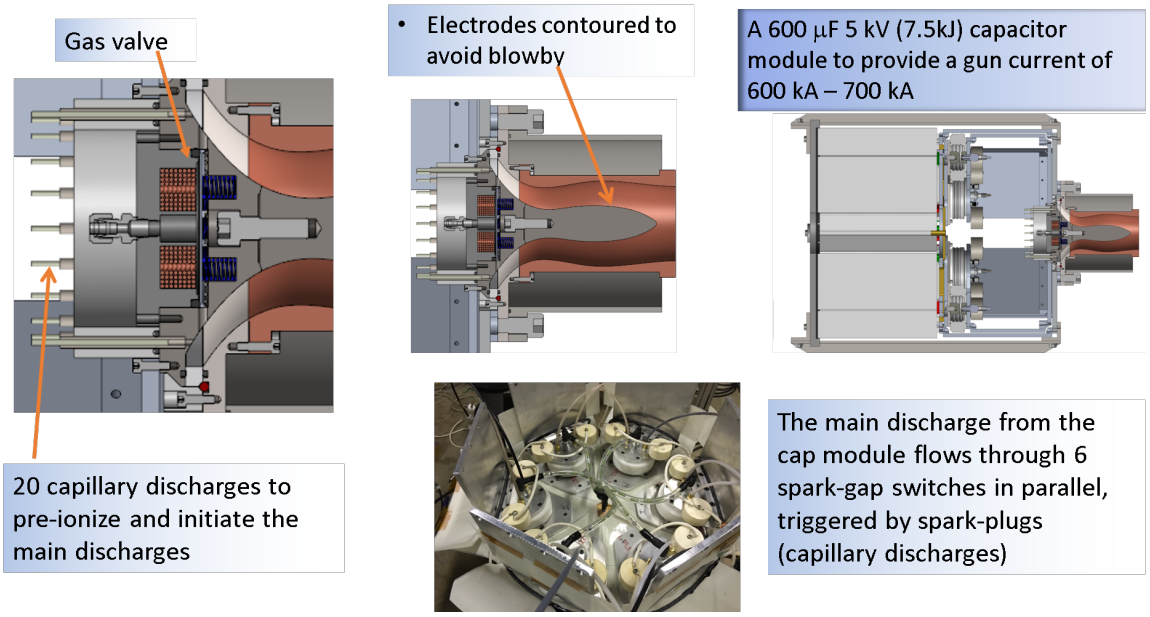

Fig. 7. Main features of the first-generation plasma gun developed under the ARPA-E ALPHA program:(a) The gas valve, (b) the pre-ionization subsystem, (c) the contoured electrodes, (d) the capacitor module and its transmission plates, (e) the spark-gap switches.

inductance transmission plates, (e) each of the capacitor submodules is connected to a spark-gap switch which is turned on by using a spark plug (trigatron), and (f) a current mixing manifold for merging the discharges of the six capacitor submodules to feed the breech of the gun. The net inductance of the pulsed power system is estimated to be ($\sim$ 16) nH. The jitter of the switches was not characterized, but was estimated to be less than 1 μs.

The plasma gun development has experienced three development cycles. The first cycle was undertaken with a series of gas valves culminating in Revision 9 (Rev9) using the ALPHA2gun. Those results have been reported elsewhere [16].The second cycle of development introduced Revision 10 (Rev10) of the gas valve, which had substantially improved performance characteristics over the first 9 versions in terms of precision gas mass metering, speed of opening and closing, reliability, and repeatability. The results reported on jet merging in this paper were achieved using the second-generation plasma gun (ALPHA2gun) equipped with the Rev10 gas valve. The performance metrics achieved by the second-generation plasma gun with the Rev10 gas valve are shown in Table III. The third cycle of the development of the plasma gun is in progress and is reported elsewhere [17].

V. REACTOR CONSIDERATIONS OF PLASMA GUNS AND CHAMBER

The design of the plasma guns and the chamber for reactor-scale applications needs to address the lifetime issues resulting from:

1. the blast from the strong point-like thermonuclear explosion creating a plasma fireball,
2. the electrode erosion due to the large pulse of current in the gun, and
3. the neutron fluence produced by the nuclear fusion micro-explosion.

Since the plasma guns are most vulnerable to neutron and plasma radiation damage, and is the more expensive part of the reactor chamber, we will begin by laying out the design envelope and maintenance option for them. The overall constraint is to develop a design envelope that will limit the cost of the plasma jet energy delivered to be below US$0.05 per MJ of energy delivered, a requirement of the ALPHA program launched by the Advanced Research Project Agency of the U.S. Department of Energy in 2015 [18]. This requirement serves to keep the overall levelized cost of electricity (LCOE) within reasonable bounds. Due to their low cost, our reactor strategy is to allow for regular replacement of the plasma guns. Most of the gun materials are recyclable or refurbishable. In an automated recycling process, we expect the recycling cost of a plasma gun to be less than that of a low-end automobile, say, US$20,000.

V.A. THE THERMONUCLEAR PLASMA FIREBALL

To set the stage for the design of the chamber and the plasma guns, we will first consider the environment in which they need to operate. Each fusion pulse is a strong micro-nuclear explosion with a plasma fireball that is propelled by 100 MJ of thermal energy from the charged fusion products and 400 MJ of neutron energy.

For the case shown in Figure 8, the ram pressure of the expanding liner may be estimated to be about 6 MPa at the radial position of 3 m. The stagnation pressure against the chamber wall will be about 4/3 times this value for an polytropic exponent of 5/3 (ratio of specific heats), giving a blast pressure of about 8 MPa, or 80 bar, for a duration of about 4 μs (thickness of the liner $\sim$1 m/liner velocity of about 250 km/s). The magnitude of the pressure is of the order of magnitude in an automobile internal combustion engine, but the duration of the pressure wave is shorter and the repetition rate is much lower (1 Hz vs 60 Hz).

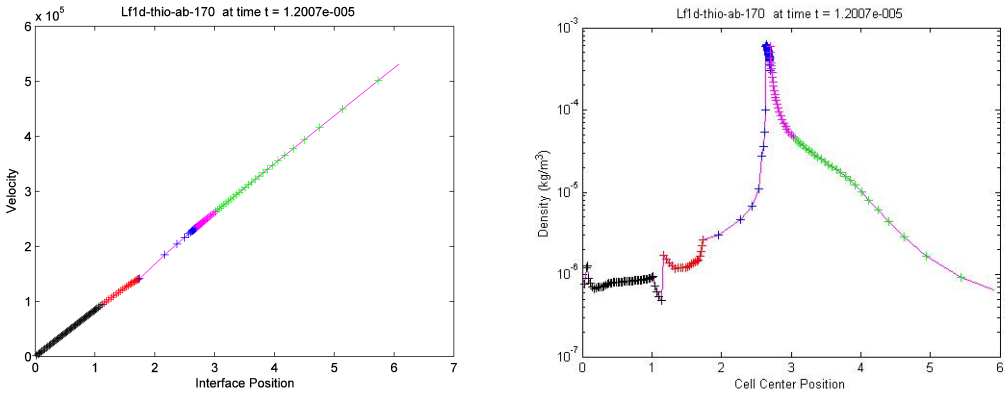

(a) (b)

Fig. 8. (a) shows the velocity profile of the plasma fireball versus radial position at an instant of time after the liner material has traveled at least 3 m. Points within the liner are indicated by the blue, magenta and green crosses. (b) shows the corresponding mass density profile. The x-axis gives the radial position, in units of meter (m) from the center of the chamber, of the 'interface' or 'cell center' of the computational node (see Appendix) at which the physical quantity is evaluated. The results are produced by the PJMIF 1D code, Lf1d, for Case #170 of Table II.

For estimating the strength of the blast from the plasma fireball in the general case, the mathematical problem is similar to the one solved by Sedov and others [19, 20, 21, 22] for a strong nuclear explosion in the atmosphere up to the point when the shock front from the blast has completely entrained the exploding liner. After that point, the dynamics of the explosion is simply one in which the relatively massive liner is accelerated by the highly energetic plasma fireball. The mathematical problem may be idealized as a dense spherical gas shell of mass M_ℓ being accelerated by a pressurized cavity created by the abrupt release of energy E_f from the fusion burn. Since the liner mass is much larger than the mass in which the fusion energy is deposited, the upper bound to the asymptotic energy of the expanding liner is E_f, and thus the upper bound to the velocity of the exploding liner is,

$$u_\ell = \sqrt{\frac{2E_f}{M_\ell}}. \tag{1}$$

Since the motion of the liner material is radial, the mass per unit solid angle of the liner remains constant. By the self-similar nature of the motion (in which the radial coordinate is a similarity variable or length scale), the thickness (Δr) of the exploding dense plasma liner is proportional to

the radial position r of the liner. By conservation of mass, the liner density ρ scales according to,

$$4\pi r^2 \rho \Delta r = M_\ell \tag{2}$$

Thus, the ram pressure scales as,

$$\rho u^2 \leq \frac{E_f}{2\pi r^2 \Delta r} = \left(\frac{r_0 E_f}{2\pi \Delta r_0}\right)\frac{1}{r^3} \tag{3}$$

where Δr_0 is the liner thickness after being processed by the blast shock wave at the radial position r_0. In a typical PJMIF scheme, $r_0 \sim 3\Delta r_0$, thus, the ram pressure and the stagnation pressure of the blast wave will be,

$$\rho u^2 \sim \frac{3E_f}{2\pi r^3},\ p_s = \left(\frac{\gamma+1}{2}\right)\rho u^2 \sim \left(\frac{\gamma+1}{2}\right)\frac{3E_f}{2\pi r^3} \tag{4}$$

within a factor of unity. For the example of Figure 8, this estimate gives a stagnation pressure of the blast wave against a first wall to be approximately 93 bar. This is the pressure which the chamber and the plasma guns need to be designed to withstand.

V.B. Electrode erosions in the plasma guns

Next, we consider electrode erosion in the guns caused by the large current pulse. An array of up to 600 guns is envisaged for the reactor to deliver a total of 10 g of plasma jets at 70 km/s. Thus, each gun is required to launch 17 mg. While the coaxial gun electrodes are contour-shaped as shown in Figure 2, to simplify the analysis, we will idealize the gun as a uniform cylindrical geometry with an average inner radius a and outer radius b and an effective acceleration length ℓ in order to estimate the current and pulse length required, and thus the electrode erosion rate.

Assuming the plasma jet is accelerated as a compact plasma slab in the mode as described in Thio [11], the electromagnetic (Lorentz) force generated by a current I in the gun acting on the plasma slab is,

$$F = \frac{1}{2}L'I^2 \tag{5}$$

where L' is the effective inductance gradient of the gun electrodes. For a cylindrical geometry with

effective inner and outer radii a and b respectively, the gun inductance gradient is given by,

$$L' = \frac{\mu}{2\pi} ln\left(\frac{b}{a}\right) \tag{6}$$

Using these expressions, the current amplitude I and pulse length Δt required are respectively:

$$I = \sqrt{m/L'\ell}\, v,\ \Delta t = \ell/v \tag{7}$$

where m and v are the mass and velocity of the plasma jet launched.

In terms of electrode erosion caused by the plasma, the inner electrode with the smaller surface area is the critical electrode to consider. It is essential that this electrode is sized to avoid any erosion caused by thermal ablation by the plasma. For tungsten, the current threshold for thermal ablation is 50 kA per cm of the perimeter of the electrode. Erosion caused by arc roots and charge transfer are largely unavoidable and available data indicate an erosion rate of less than 100 ng per Coulomb of charge transferred [23]. In Table IV, we show two possible design envelopes for the coaxial plasma gun, one with an effective plasma acceleration length of 0.5 m, the other with an acceleration length of 0.75 m, using the same dimensions for the inner and outer electrodes. For the present purpose, we will make the reasonable assumption that the effect on gun performance caused by an erosion depth of up to 10 μm (0.1% of the inner electrode diameter) will be negligible. With this assumption, the erosion-limited lifetimes of the plasma gun are between 19.6 and 23.9 million shots for the effective acceleration length ranging from 0.5 m to 0.75 m. Future experimental data is required to inform us accurately on what would be the acceptable depth of erosion before it affects significantly the gun performance.

V.C. DESIGN CONSIDERATIONS AGAINST NEUTRON DAMAGE

The effect of neutron irradiation on the performance of plasma facing components (PFC) is an ongoing research area in fusion energy development. Candidate surface cladding materials for the electrodes include tungsten and its alloys, especially W-Re alloys. Specific experimental data available on these candidate alloys at present are relatively limited, and more data are required to narrow down the design window.

The most pertinent aspect of the neutron radiation damage on the plasma guns concerns its

TABLE IV
Gun design envelop assuming an electrode erosion rate of 100 ng per Coulomb transfer at the electrode, and an acceptable erosion depth to 10 μm.

	Case 1	Case 2
Effective acceleration length	0.5 m	0.75 m
"Average" outer electrode radius	10 cm	10 cm
"Average" inner electrode radius	5 cm	5 cm
Effective inductance gradient ($\mu H/m$)	0.14	0.14
Current (MA)	1.1	0.895
Perimetric linear current density (kA/cm)	35	29
Pulse length (μs)	14.1	21.2
Net Coulomb transfer per shot (C)	15.5	19
Erosion depth per shot (pm)	0.51	0.42
Lifetime of gun electrodes (millions of shots)	19.6	23.9

effect on the mechanical strength of the electrode materials. We envisage that the design of reactor-grade gun will make use of structural metals such as steel to provide its structural strength and stability, while cladding of refractory metals such as W-Re alloys will be used to provide resistance to erosion caused by the large current and the high-temperature plasma armature accelerated.

The international standard for quantifying neutron radiation damage is displacements per atom (dpa) [24, 25]. A dose of one dpa corresponds to stable displacement from their lattice site of all atoms near absolute zero where no recovery due to thermally activated diffusion of point defects can occur. The initial number of atoms temporarily knocked off their lattice site during energetic neutron irradiation is $\sim$ 100 times the dpa value. Most of these transient displaced atoms hop onto another lattice site during the few picosecond "thermal spike" phase as their kinetic energy transferred to the displacement cascade is dissipated and the atom energies become thermalized.

For structural considerations, there are five major damage phenomena that can result in performance degradation [26]: radiation hardening and embrittlement, phase instabilities, irradiation creep, volumetric swelling from void formation (3D aggregates of vacancies), and helium embrittlement of grain boundaries causing intergranular fracture.

In existing second-generation fission reactors, structural materials are used up to a neutron irradiation fluence of $\sim$ 30 dpa. Accordingly, for the structural materials (e.g. steel) used in the construction of the plasma guns, we will limit the radiation dosage to less than 25 dpa and prescribe a design envelope of less than $0.5T_M$ for the operating temperature. Radiation hardening of tungsten and some of its alloys have been measured after they have been irradiated with neutrons

TABLE V
Plasma gun design against neutron irradiation damage

	Steel alloys	Tungsten alloys
Neutron fluence per dpa	1.4×10^{24} n/m^2	8.00×10^{25} n/m^2
Neutron fluence per shot	1.57×10^{18} n/m^2	1.57×10^{18} n/m^2
Design choice of acceptable neutron damage	25 dpa	0.5 dpa
Design lifetime in terms of shots allowed	22.3 million shots	25.5 million shots

up to 1.54 dpa [27, 28], suggesting that the metal is likely to survive mechanically this level of dpa under neutron irradiation. For the gun electrodes made of tungsten alloys, we will conservatively limit the radiation dosage to less than 0.5 dpa [27]. When these neutron damage levels are reached, the plasma guns are replaced.

For the baseline reactor performance shown in Table I, the total neutron yield is 400 MJ or 1.771×10^{20} per shot. The neutron fluence (neutrons per unit area) on a chamber wall of 3 m radius is $1.57 \times 10^{18} n/m^2$ per shot. For steel alloys, the neutron fluence to cause a 1 dpa radiation damage is $1.396 \times 10^{24} n/m^2$ [26]. 25 dpa of neutron damage in the steel structural elements in the plasma guns will require 22.3 million shots. Tungsten alloys can withstand a neutron dose of $8 \times 10^{25} n/m^2$ (with neutron energy 0.1 MeV) before 1 dpa of damage is caused. For the plasma gun electrodes made of tungsten alloys, they will withstand 25.5 million shots before they need to be replaced when 0.5 dpa damage is caused. (Table V).

VI. EXPERIMENTS ON JET MERGING AND THE FORMATION OF A CONICAL SECTION OF A PLASMA LINER: STATUS REPORT

VI.A. The Experimental Platform

An experimental platform (PLX), Fig. 9, for exploring the physics of the formation of a spherical plasma liner by the merging of a spherical array of hypersonic plasma jets is being developed at the Los Alamos National Laboratory, jointly by HyperJet Fusion and Los Alamos National Laboratory. While up to 60 plasma guns may be installed on the spherical chamber, the first experiment will involve only 36 guns. The objectives of this first experiment on plasma liner formation are: (1) to assess effects of discrete jet merging on liner Mach number and non-uniformity, (2) to demonstrate fully spherical plasma-liner formation and convergence scaling of liner peak ram pressure and non-uniformities, (3) to benchmark computational modeling of the

Fig. 9. The PLX-α experiment being jointly developed by HyperJet Fusion and Los Alamos National Laboratory, funded by ARPA-E and Strong Atomics, LLC. Up to 36 guns are expected to be fielded in 2019.

merging of hypersonic plasma jets and the formation of a spherical plasma liner by a suite of codes. It is the world's first experimental facility for studying the interactions of multiple hypersonic plasma jets.

The experiment is designed based on the physics criteria for a subscale experiment to address issues relevant to a fusion-scale plasma liner that must reach 100-Mbar peak ram pressure [29, 9]. These physics criteria include: (1) The liner must be hypersonic, high-Z (nitrogen and above), with effective polytropic index γ less than 5/3 to model the radiative/EOS effects of Kr or Xe, (2) Mach number M of the liner greater than 10, liner speeds exceeding 50 km/s, and (3) jet merging must be in a collisional regime. These criteria imply a minimum liner kinetic energy of 65 kJ (260 kJ stored electrical energy) and up to 50-mg liner mass (when using Xe) at 50 km/s.

Since late 2016, more than 3,500 shots have been taken at the PLX facility, Fig. 10. Experiments have been performed investigating the physics of the merging of hypersonic plasma jets involving 2 to 7 jets [16, 30]. The suite of diagnostics available to these experiments are listed in Table VI.

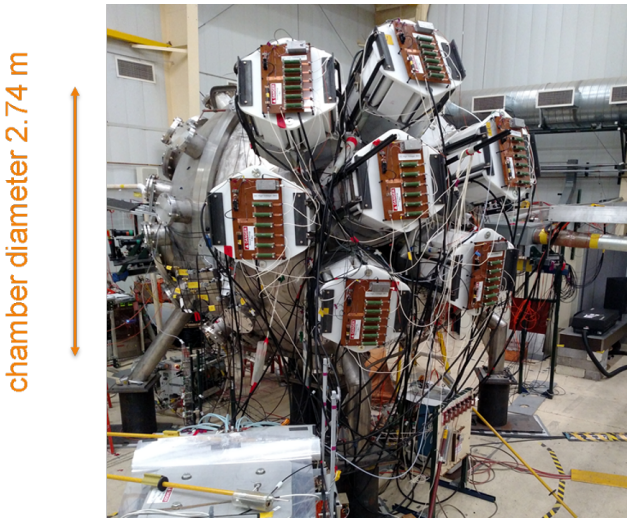

Fig. 10. The PLX facility at Los Alamos National Laboratory: 7 guns mounted, photo taken on July 2, 2018. Up to 60 guns may be mounted

TABLE VI
Diagnostics available on PLX

Diagnostics	Measurements
Multi-chord interferometry	7 chords end-on, 5 chords side-on Density uniformity 2-jet and 3-jet plasma shock profile merged jet length
Survey spectroscopy	Electron temperature and ionization state Characterization of plasma impurities
High resolution spectroscopy	Ion heating and Mach number degradation
2-chord photodiodes	Exit velocity of plasma jets Jet-to-jet coherence of jets
Single and multi-frame high-speed imaging	Jet-to-jet coherence Plasma shock profile

TABLE VII
The suite of computer codes used to support the experimental development

Problem modeled	Codes	Issues addressed
Coaxial gun component technology development	gv	gas valve, gas injection
Coaxial gun design and optimization	MACH2 (2D rad-MHD) SPFMax (3D SPH)	Electrode contour design, capacitor module sizing
PLX-relevant experiments (3D, 2 - 60 guns)	SPFMax (3D SPH), FronTier (3D front-tracking hydro)	Jet merging physics, non-uniformity, and ram-pressure scaling effects of jet-to-jet variations
Liner compressing a magnetized target plasma (1D and 2D)	USim, FLASH	Achievable energy gain, stability/transport in magnetized target Rayleigh-Taylor instabiity at the liner/target interface
Formation of $\beta > 1$ target plasma via merging magnetized plasma jets	FLASH, LA-Compass	Are there appropriate λ_{gun} (current/flux ratio) values of merging, magnetized plasma jets that lead to transient $\beta > 1, \omega\tau > 1$ conditions?

VI.B. Theoretical, computational support, and status of experimentation

A suite of computer codes is used to support the development of the PLX-α liner formation experiment as shown in Table VII. The design and development of the Revision 10 gas valve is supported by a semi-analytic 1D code (gv) using a MatLab platform. The development of the gun electrode contours and the sizing of the driving capacitor module was accomplished with the help of the MACH2 2D radiative hydrodynamic code [15] and the University of Alabama 3D Smoothed Particle Hydrodynamics (SPH) code, SPFMax [31]. The jet-merging and liner formation are modelled using the 3D SPFmax code and the Brookhaven National Laboratory 3D FronTier front-tracking code [32]. Radiative magnetohydrodynamics (rad-MHD) modelling of the liner compressing a magnetized plasma in 1D and 2D are modelled by the codes USim and FLASH. Formation of $\beta > 1$ target plasma via the merging of magnetized plasma jets are studied with the help of FLASH and LA-Compass.

Details of simulations and the computational studies of the dynamics in jets merging are given in [10, 33]. When the jets merge, shocks are formed at the interface between the jets. These are the primary shocks, which proceed to process the body of the jets laterally with time. The array of flows that have been processed by the primary shocks merge to cause the next generation of interfacial shocks, the secondary shocks.

Extensive experimental campaigns were conducted using 6 jets and 7 jets arranged in a conical array. The experimental results were compared with the numerical simulations. The Brookhaven National Laboratory FronTier code was used to model the experiments with synthetic diagnostics that simulate the fast-framing camera for two cases of jet-to-jet variations in mass and variations in timing [10]. In one case, the effects of random jet-to-jet mass variations of up to 5% is simulated. In the second case, the effects of jet-to-jet mass variations up to 10%, and the random jet-to-jet timing variations up to 2μs are simulated. Comparing the computational results with the experimental ones suggest that the plasma jets produced by the second generation of plasma gun (the ALPHA2gun) with the Rev10 gas valve may be subject to variations as large as the ones simulated with random jet-to-jet variations in mass of up to 10%, and timing variations of up to 2μs.

For a near-term 60-gun liner formation experiment on the PLX platform, 2-temperature (ion and electron) SPFMax 3D SPH simulations have been performed to elucidate the shock heating of the liner caused by the deflection of the hypersonic flows during the merging of the jets. Details of the studies will be presented in an upcoming paper [30].

The simulation studies indicate that there is sufficient time for the ions to be cooled by the electrons during the radial convergence of the plasma liner. Consequently, the ion Mach number manages to recover during the electron-ion equilibration time to stay over an average value of 10 at the end of the electron-ion equilibration time. Two-jet merging experiments at PLX borne out this theoretical and computational expectation. Details of the experiments and the analysis of the data are presented in [34] and also in an upcoming paper [30].

VII. SUMMARY

In this paper, the fusion concept, Plasma-Jet Magneto-Inertial Fusion (PJMIF), is described and a status report on its development is presented. Development of the first experiment to explore the formation of a spherical plasma liner by the merging of a spherical array of 36 plasma jets is in progress. Plans in the near future includes development of a suitable target for PJMIF and implosion of a target by a spherical plasma liner to demonstrate target heating.

A. APPENDIX: BRIEF DESCRIPTION OF THE LF1D CODE

Lf1d is a MATLAB code for modeling plasma dynamics using a Lagrangian approach, in which the computational cells and interfaces move with the fluid. In Lf1d, the kinematic equation relating the position of a mass particle to its velocity is the equation of continuity. The Euler equation is used as the momentum equation, and the first law of thermodynamics as the energy equation. Discretising these equations of continuity, momentum and energy yield a set of ODE's for the positions of the mass elements, their velocities and internal energies. Lf1d integrates the resultant set of ODE's explicitly in time by using a Runge-Kutta-Fehlberg routine which is 4-1/2-order with error control. Richtmyer-Neumann pseudo-viscosity is used to stabilize the time integration of the equations. Fusion reactions are modeled in the target and afterburner. The computational domain is divided into a number of blocks. Each block is further divided into a number of computational cells. For each block, alpha energy deposition is treated by specifying a fixed fraction of the alpha energy to be deposited locally or non-locally with the residual being propagated outward radially from one computational block to the next block (target to afterburner, afterburner to liner).

Planar, cylindrical and spherical geometries are provided. The physical domain is mapped into computational domain as a line of ordered cells, designated as cell $2, \ldots, (n_f - 1)$. These cells are bounded by $(n_f - 1)$ interfaces. Thus cell (i) is bounded by interface(i) and interface(i+1). A physical quantity v associated with the interface(i) is denoted with the subscripted variable v_i. A physical quantity q associated with the center of the cell(i) is denoted as $q_{i+1/2}$. With the symbols, r, u, ρ, p, q, V, A, and ϵ having their usual meanings of position coordinates, velocity, density, pressure, heat, cell volume, area of interface and internal energy respectively, the discretised equations of continuity, momentum and energy are taken to be,

$$\frac{dz_i}{dt} = u_i \tag{8}$$

$$\left(\frac{d\mathbf{u}}{dt}\right)_i = \frac{p_{i+1/2} - p_{i-1/2}}{\langle \rho \Delta r \rangle_i}, \langle \rho \Delta r \rangle_i = \rho_{i-1/2}\left(r_i - r_{i-1/2}\right) + \rho_{i+1/2}\left(r_{i+1/2} - r_i\right) \tag{9}$$

$$\left(\frac{d\epsilon}{dt}\right)_{i+1/2} = \left(\frac{dq}{dt}\right)_{i+1/2} - \left(p\frac{dV}{dt}\right)_{i+1/2} \tag{10}$$

The pdV work by cell (i) is computed in the form,

$$\left(p\frac{dV}{dt}\right)_{i+1/2} = p_{i+1/2}\left(-u_i A_i + u_{i+1}A_{i+1}\right) \tag{11}$$

The computaional domain is typically subdivided into a number of blocks. Each block is in turn subdivided into a number of Lagrangian cells, to which the above equations of continuity, momemtum and energy are applied. The block closest to the origin simulates the target plasma, the next outer block simulates the afterburner. This is typically followed by three more outer blocks simulating the imploding liner. Each block is discretized independently. Typically the target plasma is modelled with more than 100 cells, the afterburner about 50 cells, and the liner another 200 cells.

ACKNOWLEDGMENTS

This work is supported by Strong Atomics, LLC and the ARPA-E ALPHA Program under contract DE-AR0000566.The PJMIF approach has been selected for development under the ARPA-E ALPHA program. Over the last three years, under the ALPHA program, HyperJet Fusion/HyperV Technologies together with Los Alamos National Laboratory, have been developing the Plasma Liner Formation Experiment (PLX-α) at Los Alamos to explore the physics and demonstrate the formation of a spherical liner by the merging of a spherical array of plasma jets. Development of the first experiment to explore the formation of a spherical plasma liner by the merging of a spherical array of 36 plasma jets is in progress, being undertaken jointly by Los Alamos National Laboratory and HyperJet Fusion Corporation, with support from the U.S. Department of Energy Advanced Research Project Agency (ARPA-E) and Strong Atomics, LLC.

REFERENCES

[1] I. R. Lindemuth and R. E. Siemon, "The fundamental parameter space of controlled thermonuclear fusion," *Amer. J. Phys.*, **77**, 407 (2009).

[2] Y. C. F. Thio, E. Panarella, R. C. Kirkpatrick, C. E. Knapp, F. Wysocki, P. Parks, and G. Schmidt, "Magnetized Target Fusion in a Spheroidal Geometry with Standoff Drivers," E. Panarella (Editor), *Current Trends in International Fusion Research– Proceedings of the Second International Symposium*, 113, National Research Council of Canada, Ottawa.

[3] S. C. Hsu, T. J. Awe, S. Brockington, A. Case, J. T. Cassibry, G. Kagan, S. J. Messer, M. Stanic, X. Tang, D. R. Welch, and F. D. Witherspoon, "Spherically Imploding Plasma Liners as a Standoff Driver for Magnetoinertial Fusion," *IEEE Trans. Plasma Sci.*, **40**, 1287 (2012).

[4] C. E. Knapp and R. C. Kirkpatrick, "Possible energy gain for a plasma-liner-driven magneto-inertial fusion concept," *Phys. Plasmas*, **21**, 070701 (2014).

[5] S. C. Hsu and S. J. Langendorf, *J. Fusion Energy*, **38**, 182 (2018); https://doi.org/10.1007/s10894-018-0168-z.

[6] Y. C. F. Thio, Rapid scan of the parameter space for PJMIF using an idealized Lagrangian 1D fluid code LF1D, unpublished report, U.S. Department of Energy, Germantown, MD, 2011.

[7] S. J. Langendorf and S. C. Hsu, "Semi-analytic model of plasma-jet-driven magneto-inertial fusion," *Phys. Plasmas*, **24**, 032704 (2017).

[8] W. L. Barr, R. J. Burleigh, W. L. Dexter, R. W. Moir, and R. R. Smith, "A Preliminary Engineering Design of a 'Venetian Blind' Direct Energy Converter for a Fusion Reactor," *IEEE Trans. Plasma Science*, **2**, 71 (1974).

[9] Y. C. F. Thio, C. E. Knapp, R. C. Kirkpatrick, R. E. Siemon, and P. J. Turchi, "A Physics Exploratory Experiment on Plasma Liner Formation," *J. Fusion Energy*, **20**, 1 (2001).

[10] W. Shih, R. Samulyak, S. C. Hsu, S. J. Langendorf, K. C. Yates, and Y. C. F. Thio, "Simulation Study of the Influence of Experimental Variations on the Structure and Quality of Plasma Liners," *Phys. Plasmas*, **Accepted for publication**, pages TBD (2018).

[11] Y. C. F. Thio, J. T. Cassibry, and T. E. Markusic, "Pulsed Electromagnetic Acceleration of Plasmas," Paper AIAA-2002-3803 presented at the 38th AIAA/ASME/SAE/ASEE Joint Propulsion Conference & Exhibit, Indianapolis, IN, July 7–10, 2002.

[12] J. T. Cassibry, Y. C. F. Thio, and S. T. Wu, "Two-dimensional axisymmetric magneto-hydrodynamic analysis of blow-by in a coaxial plasma accelerator," *Phys. Plasmas*, **13**, 053101 (2006).

[13] Y. C. F. Thio, Magneto-inertial fusion: An emerging concept for inertial fusion and dense plasmas in ultrahigh magnetic fields, in Proc. Fifth International Conference in Inertial Fusion Sciences and Applications, Kobe, Japan, 2007; http://www.osti.gov/scitech/biblio/1159661.

[14] Y. C. F. Thio, "Status of the U.S. Program in magneto-inertial fusion," *J. Physics Conference Series*, **112**, 042084 (2008).

[15] F. D. Witherspoon, A. Case, S. J. Messer, R. Bomgardner II, M. W. Phillips, S. Brockington, and R. Elton, "A contoured gap coaxial plasma gun with injected plasma armature," *Rev. Sci. Instrum.*, **80**, 083506 (2009).

[16] S. C. Hsu, S. J. Langendorf, K. C. Yates, J. P. Dunn, S. Brockington, A. Case, E. Cruz, F. D. Witherspoon, M. A. Gilmore, J. T. Cassibry, R. Samulyak, P. Stoltz, K. Schillo, W. Shih, K. Beckwith, and Y. C. F. Thio, "Experiment to Form and Characterize a Section of a Spherically Imploding Plasma Liner," *IEEE Trans. Plasma Sci.*, **46**, *99*, 1951 (2018).

[17] Y. C. F. Thio, F. D. Witherspoon, S. Brockington, A. Case, E. Cruz, and M. Luna, "Coaxial Plasma Gun Development for Plasma-Jet-Driven Magneto-Inertial Fusion (PJMIF)," *Bull. Amer. Phys. Soc.*, **DPP**, BM9.00002 (2018).

[18] United States Department of Energy Advanced Research Project Agency: ALPHA Program Overview. https:arpa-e.energy.gov/sites/default/files/documents/files/ALPHA_ProgramOverview.pdf. (2015).

[19] S. I. Sedov, *Similarity and Dimensional Methods in Mechanics, English translation, (M. Holt, ed.)*, Academic Press, N.Y.

[20] S. I. Sedov, *Propagation of Strong Blast Waves*, vol. 10, Prikl. Mat. iMekh (1946).

[21] G. I. Taylor, *Proc. Roy. Soc. (London), Ser. A*, **201**, 175 (1950).

[22] G. Chernyi, "The problem of point explosion," *Dokl. Akad. Nauk SSSR*, **112**, 213 (1957).

[23] M. Tanaka, T. Ikeba, Y. Liu, S. Choi, and T. Watanabe, "Investigation of Electrode Erosion Mechanism of Multi-Phase AC Arc by High-Speed Video Camera," *J. Physics: Conf Series*, **441**, 012015 (2013).

[24] S. J. Zinkle and B. N. Singh, *J. Nucl. Mater.*, **199**, 173 (1993).

[25] M. J. Norgett, M. T. Robinson, and I. M. Torrens, *Nucl. Eng. Des.*, **33**, 50 (1970).

[26] S. J. Zinkle, "Fusion materials science: Overview of challenges and recent progress, Phys. Plasmas," **12**, 058101.

[27] T. Tanno, M. Fukuda, S. Nogami, and A. Hasegawa, "Microstructure Development in Neutron Irradiated Tungsten Alloys," *Materials Transactions*, **52**, 1447 (2011).

[28] A. Hesegawa, M. Fukuda, T. Tanno, and S. Nogami, "Neutron Irradiation Behavior of Tungsten," *Materials Transaction*, **54**, 466 (2013).

[29] S. C. Hsu and Y. C. F. Thio, "Physics Criteria for a Subscale Plasma Liner Experiment," *J. Fusion Energy*, **37**, 103 (2018).

[30] K. C. Yates, S. J. Langendorf, S. C. Hsu, J. P. Dunn, M. Gilmore, S. Brockington, A. Case, E. Cruz, F. D. Witherspoon, Y. C. F. Thio, J. T. Cassibry, R. Samulyak, K. Schillo, and W. Shih, "Experimental characterization of a section of a spherically imploding plasma liner formed by merging six or seven hypersonic plasma jets," **in preparation**.

[31] J. T. Cassibry, R. Cortez, C. Cody, S. Thompson, and L. Jackson, "Three Dimensional Modeling of Pulsed Fusion for Propulsion and Terrestrial Power Using Smooth Particle Fluid with Maxwell Equation Solver (SPFMaX)," *53rd AIAA/SAE/ASEE Joint Propulsion Conference, AIAA Propulsion and Energy Forum.*

[32] R. Samulyak, P. Parks, and L. Wu, "Spherically symmetric simulation of plasma liner driven magnetoinertial fusion," *Phys. Plasmas*, **17**, 092702 (2010).

[33] J. T. Cassibry, K. J. Schillo, R. V. Samulyak, S. C. Hsu, and Y. C. F. Thio, "Effects of plasma jet initial conditions and number on peak ram pressure and uniformity for plasma jet driven magneto-inertial fusion experiments on PLX-α," *Bull. Amer. Phys. Soc.*, **DPP18**, http:meetings.aps.org/Meeting/DPP18/Session/GP11.133 (2018).

[34] S. Langendorf, "Experimental Measurements of Ion Heating in Collisional Plasma Shocks and Interpenetrating Supersonic Plasma Flows," *Bull. Amer. Phys. Soc.*, **DPP18**, meetings.aps.org/Meeting/DPP18/Session/YI3.2 (2018).